Scholar Publishing Group
International Journal of Engineering Technology and Construction
https://doi.org/10.38007/IJETC.2022.030205
ISSN 2789-7176 Vol. 3, Issue 2: 62-82

Carbon Raw Materials on the Properties of Al2O3-SiC-C Iron Trough Casting Building Materials

Cranig Pearsanll*

BA Components Ltd, UK

**corresponding author*

Keywords: Carbon Raw Materials, PID Control, Al2O3-SiC-C Refractories, Iron Trough Castables, Mathematical Models of Steel

Abstract: A large number of studies have shown that the addition of carbon raw materials will have a great impact on the fluidity and construction performance of calcium aluminate cement (CAC) combined with castables. In order to explore the impact of carbon raw materials on performance when used in Al2O3-SiC-C iron ditch castables, this paper uses site measurement, experimental equipment collection and result subdivision methods to collect data, streamline the algorithm and use the algorithm to better clarify the influencing factors. And design a theoretical result that can cover its influencing factors. Through microscopic inspection, the X-ray diffraction (XRD) images of the two sets of samples with 0.8% and 6.8% carbon content after heat treatment at 1050℃ and 1500℃ were studied. The results showed that the X-ray diffraction (XRD) images with 0.8% carbon content were compared with carbon. The main crystalline phases of the W group samples with a content of 6.8% are corundum and SiC. After heat treatment at 1500℃, the sample with 6.8% carbon content has a higher main peak of SiC than the sample with 0.8% carbon content. , Indicating that as the carbon content increases, more SiC is formed in the sample. Further exploring the high-temperature flexural strength of the sample after heat treatment at 1500℃, we can find that when the carbon addition is 4.7%, the high-temperature flexural strength of the sample has a maximum value of 2.8MPa. With the increase of the carbon addition, the sample the high temperature flexural strength has been improved. It has basically realized the combination of theory and practice, and obtained the available research results.

1. Introduction

At present, the $Al_2O_3 - SiC - C$-type castable has been widely used as the working layer material of the domestic large and medium-sized blast furnace tap ditch. The traditional tap

ramming material mainly uses alumina, silicon carbide and carbon or coke as raw materials, and a certain amount of water is added. It is made by wet mixing and stirring. In actual use, it must be baked before tapping. The strength is not high, the service life is short, and the number of trench repairs affects the production efficiency. $Al_2O_3 - SiC - C$-quality castables have the characteristics of high strength, good thermal shock stability, excellent wear resistance and corrosion resistance. Compared with traditional ASC ramming materials, the service life and iron capacity are greatly improved.

However, with the development of modern iron product technology and technological innovation, the use of $Al_2O_3 - SiC - C$-type casting materials has become more complex, requiring not only corrosion resistance at high temperatures, but also separation analysis and peeling caused by reactions. At the same time, environmental protection problems have also been solved, and the requirements for the use and efficiency of stainless steel materials are getting higher and higher. Therefore, extending the service life of stainless steel materials, increasing the strength of metals, and reducing maintenance losses and repair times are important issues that need to be explored and identified in actual production. The combination and addition of carbon raw materials is a good research guide for solving the functional changes of building materials and improving current problems.

The research on carbon raw materials is now quite mature, and the related research on the performance of iron ditch pouring building materials has also been considerable. In 2017, Papailias F studied the periodicity of the Baltic Dry Bulk Index (BDI) Characteristics and their impact on predictive performance. In their forecasting exercises, they showed that commodities and triangular regression can improve forecasts, then use their forecast results for investment exercises and show how they can be used to improve risk management in the freight department. However, the performance studied here cannot be equal to the performance of building materials [1]. In 2019, Hasa B said that the front cover demonstrated the operation of the polymer electrolyte membrane fuel cell (PEMFC) during the hydrogen supply period. The metal phase of the electrode (usually Pt and Ru) is usually dispersed on a carbon-based support. He uses new carbon materials (such as carbon nanotubes, biochar and graphene) as an alternative carrier and compares it with the most advanced Vulcan XC-72. Unfortunately, the depth of research is still not enough [2]. In 2016, Fayomi O used electrodeposition technology to prepare Zn-SiC and Zn-Al2O3-SiC composite coatings in a sulfate bath. The resulting composite coating is performed by adding Al2O3/SiC particles to the zinc-containing bath. The results show that the hardness, thermal stability and corrosion resistance of Zn-Al2O3-SiC have been significantly improved compared to the Zn-SiC coating substrate. This is due to the dispersion strengthening effect and grain induction effect of Al2O3/SiC particles. However, there are errors in the research process [3]. In 2019, Pugalenthi P produced four samples with different compositions, including SiC (3, 5, 7 and 9 w/%) and Al w/% in all combinations. The test results show that the increase of the w/ % fraction of the reinforcing material leads to the increase of the tensile strength, yield strength and hardness of the aluminum composite material, but the percentage of elongation decreases with the addition of ceramic particles. Unfortunately, the research results failed to meet expectations [4]. In 2020, Shivakumar H showed that excellent GNPs fillers are reinforced to epoxy matrix and carbon fiber/epoxy hybrid composite panels to enrich their mechanical properties. Graphene nanosheets of 0.5, 1, 1.5, and 2 weight percent were integrated into epoxy resin, and physical and mechanical properties (microstructure, density, tensile, bending, and impact strength) were studied. But there is no good description of the research conclusions [5]. In 2017, in order to improve the performance of the force sensor of the substrate material, Shuaizhen LI mixed different types of carbon fillers

(acetylene black, superconducting carbon black, multi-walled carbon nanotubes, nano graphite) into polyether-polyol polyurethane through physical blending. The research results show that acetylene black has the best dispersibility in the substrate. However, the research conclusions are poor in practicability and cannot be applied on a large scale [6]. In 2018, P. W U used plasma treatment to modify the surface of multi-walled carbon nanotubes (MWCNT). Scanning electron microscope (SEM), transmission electron microscope (TEM), energy dispersive X-ray analysis (EDX) and X-ray diffraction (XRD) were used to study the microstructure of cermets prepared with different additions of MWCNTs. Cermets with 0.5 wt% MWCNTs showed the highest TRS and fracture toughness. However, the research content is not rich enough to support the research conclusion [7].

The innovations of this article are: (1) The importance of the aluminum industry and the problems in the domestic rotary kiln carbon satin burning process are analyzed, and the research status is explained in combination with the actual situation; (2) The process mechanism of the rotary kiln burning process is emphasized. , And the main factors affecting the satin-burning temperature, the algorithm framework of the automatic control system of the material is proposed; (3) The carbon content, that is, the influence of the amount of carbon added on the structure and performance of the $Al_2O_3 - SiC - C$ castable is analyzed. Through the above work, the research content of this article is more extensive and can provide a wide range of support.

2. Method Based on the Influence of Carbon Raw Materials on the Properties of $Al_2O_3 - SiC - C$ Iron Trough Castable Materials

2.1. Carbon Raw Materials

The basic process of carbon production includes: raw material preparation, raw material roasting, material mixing and blending, green burning and anode assembly. Calcining is an important process in the production of coal products. During the satin burning process, the carbon-containing raw materials undergo a significant change from the basic composition to the system structure. As a product of the oxidation process, the tar immediately after the reaction determines the quality of the anode and the behavior of the anode in the electrode element, which in turn affects the metabolic function and systemic benefits of the electrode battery [8].

The purpose of calcination is to make the material undergo a series of physical and chemical changes under high temperature conditions, thereby eliminating moisture changes in the raw materials, increasing the weight and mechanical strength of the raw materials, and improving the strength and chemical stability. Promote the evaporation of the monomer carbon in the raw materials and the accumulation of sulfur, so that the physical and chemical properties of the raw materials after combustion are significantly improved [9].

Calcination is the main process of anode production [10]. Rotary kilns are widely used in modern carbon fiber combustion processes due to their simple method, high output, high degree of mechanization, and strong raw material improvement. The firing temperature is the key to determining the quality of the synthesized coke [11]. The material flow in the whole process is shown in Figure 1 [12].

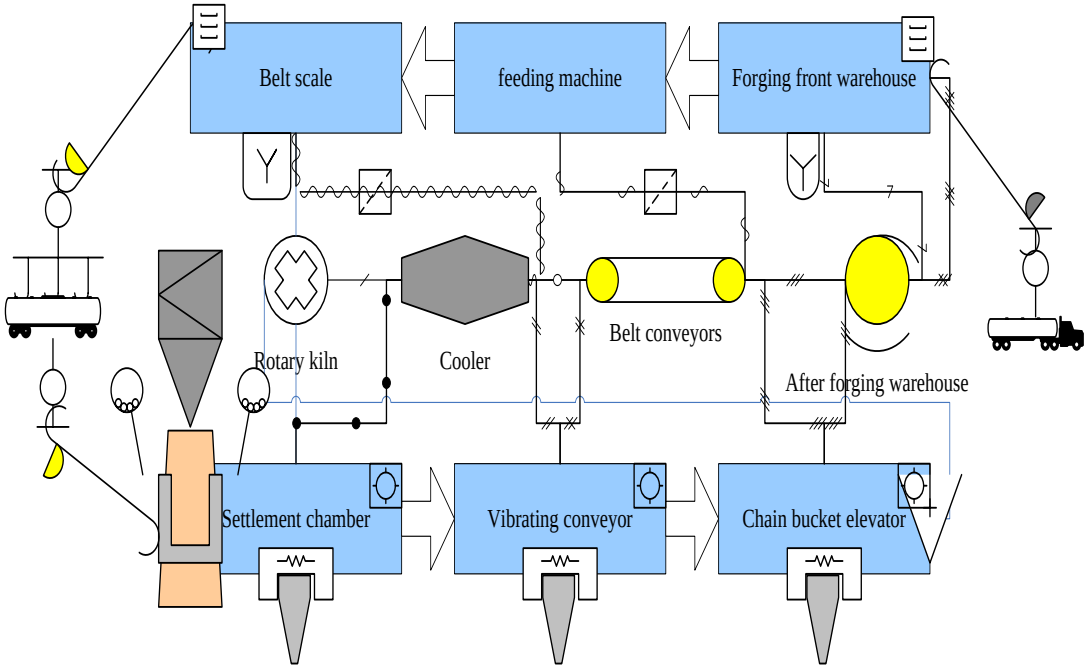

Figure 1. The material flow of the calcining process

As shown in Figure 1, the tar enters the next calciner after three initial stages of cooling and freezing, and is finally released as a petroleum coke product. For an overview of vaporized gases at different temperatures, it was shown in Table 1 [13].

Table 1. Composition of volatile matter at different temperatures

Project Temperature	CO_2	CO	H_2	CH_4
550	2.5	9.1	8.7	0.5
600	0.5	13.8	62	9.1
650	0.6	7.8	84	1.7
700	0.3	3.5	92	0.1
750	0.05	1.8	93	0.2

The carbon raw material has undergone significant physical and chemical changes during the satin firing process, forming many physical and chemical properties, which can meet the requirements of the production of default anodes. However, under different processes or conditions, there are differences in the quality of petroleum coke, that is, the quality of petroleum coke and many technical and economic indicators in the calcination process. To improve these data, it is necessary to increase the efficiency of the rotary kiln and improve the technical level of the production process. [14].

In the process of satin-firing raw materials in the rotary kiln, the temperature of the calcination zone will be affected by various process variables and become unstable, thereby affecting the quality of the forged coke. Among these variables, the satin-burning temperature has the greatest influence on the feed rate [15]. Figure 2 shows a schematic diagram of quantitative control when the feeding system conveys materials.

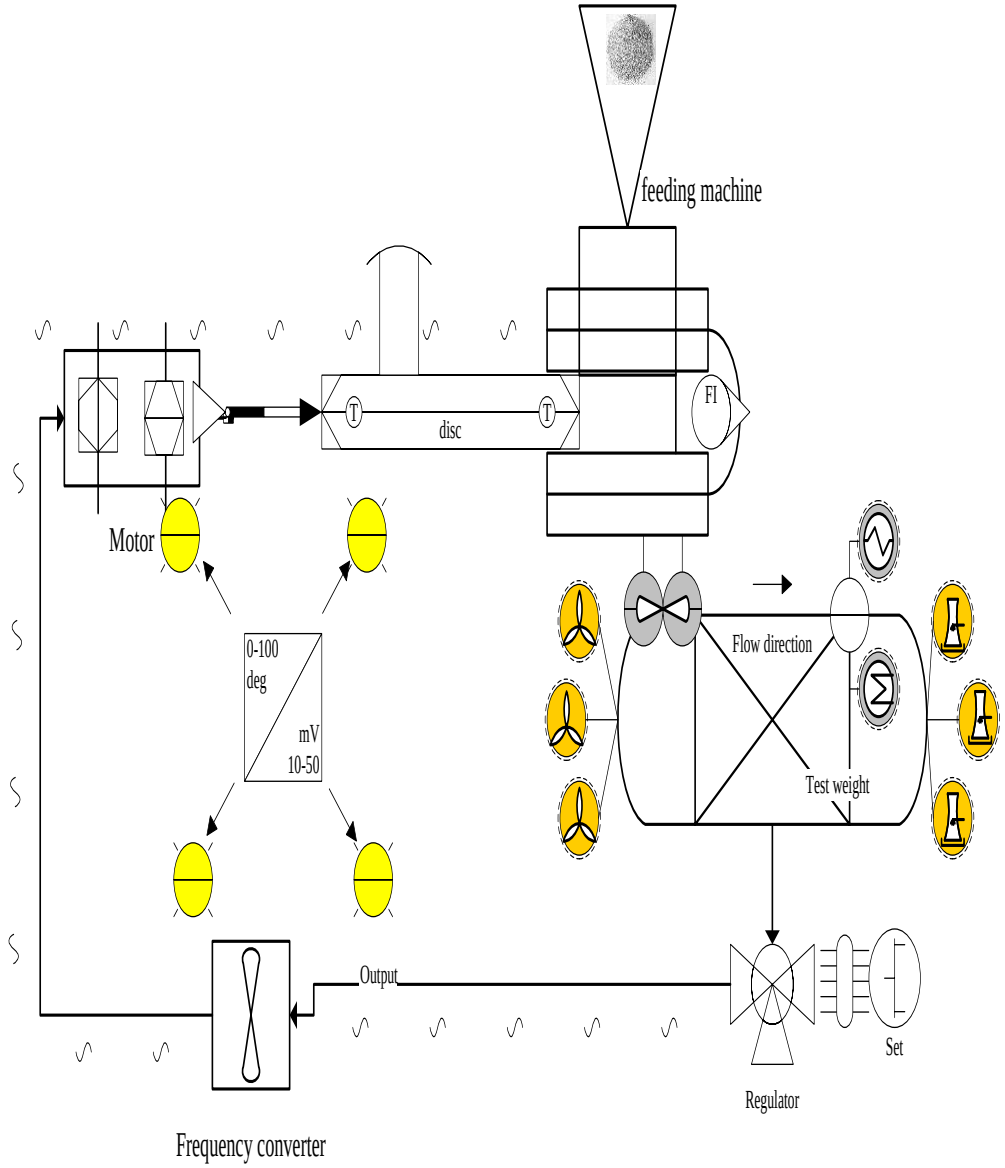

Figure 2. Schematic diagram of automatic feeding control system

It can be seen from Figure 2 that the average application size of the system is achieved by adjusting the speed of the disc feeder. The PID control system is simple, with clear physical structure, strong adaptability, high stability, and high reliability. The system design has a strong technical foundation and can be applied to different control methods. It is most commonly used for process control [16]. Practical work experience and scientific analysis show that the control algorithm has excellent improvements and capabilities for a large number of enterprise objects, and can achieve the required control function indicators [17]. Based on the actual work of this example, PID control can be used to detect the addition of carbon raw materials.

The typical PID control structure is shown in Figure 3 [18].

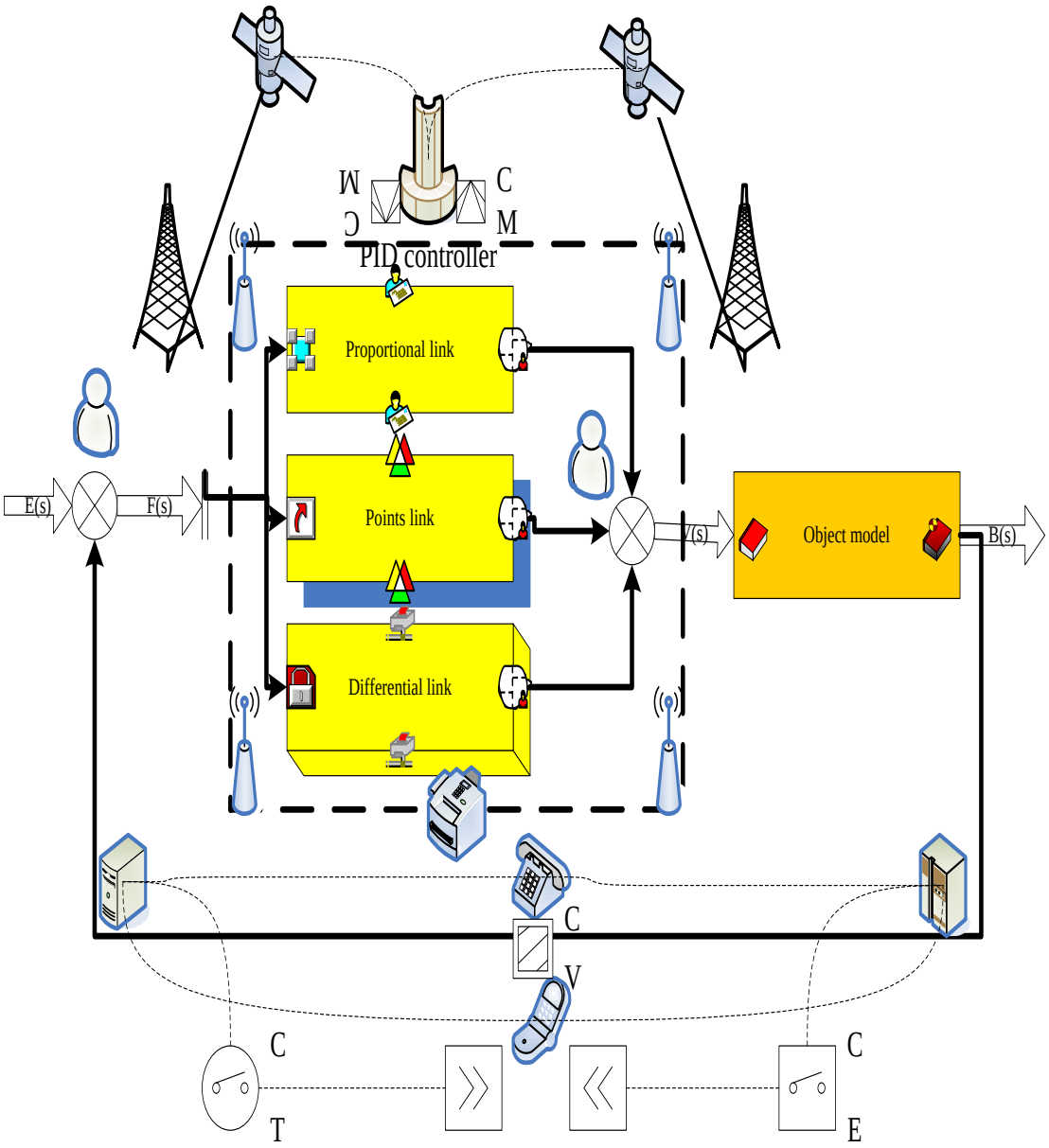

Figure 3. Typical PID control structure

It can be seen from Figure 3 that it is a linear controller;

$$f(s)=e(s)-b(s)-y(s)\sum_{e_l}^{u=1}(u_a+u_b) \tag{1}$$

The proportional q, integral u and derivative w of the deviation are combined to form a control quantity through a linear combination to control the controlled object, so it is called a controller. Its control law is;

$$v(s)=g_q\left[f(s)+\frac{1}{s_1}\int f(\rho)w\rho+s_w\frac{wf(s)}{ws}\right] \quad (2)$$

In the formula, g_q is the proportional coefficient; s_1 is the integral time constant; w_s is the derivative time constant. The form of the discrete equation is;

$$v(g)=g_q*f(g)+g_1*\sum_{k=0}^{g}f(k)+g_w*[f(g)-f(g-1)] \quad (3)$$

$$g_1=g_q s/s_1, g_w=g_q s_w/s \quad (4)$$

It can be seen from Equation 4 that the integral term is a function of all error terms from the first sampling period to the current sampling period, the differential term is a function of the current sampling and the previous sampling, and the proportional term is only a function of the current sampling, and its expression is ;

$$\nabla v(g)=v(g)-v(g-1) \quad (5)$$

$$\Delta v(g)=g_q*[f(g)-f(g-1)]+g_1*f(g)+g_w*[f(g)-2f(g-1)+f(g-2)] \quad (6)$$

Among them; v(g) represents the output value of the computer at the gth sampling time; f(g) represents the deviation value input at the gth sampling time. In the above formula, g_q represents the proportional coefficient, g_1 represents the integral coefficient; g_w represents the differential coefficient [19].

In the computer control system, the control law is realized by the computer program, so it has great flexibility. Some problems that could not be realized in the analog controller can be solved after the introduction of the computer, so a series of improved algorithms are produced to meet the needs of different control systems.

(1) Integral Separation Control Algorithm

The idea of integral separation is that when the absolute value of the deviation is greater than a certain set value, the integral does not work; when the deviation is small, the integral function is introduced to improve the performance of the adjustment section. The introduction of integral separation control algorithm not only maintains the integral effect, but also reduces the overshoot, which greatly improves the control performance. Its specific implementation is as follows;

$$\lambda=\begin{cases}0.1 & when|f(g)|>\phi\\ 0.9 & when|f(g)|<\phi\end{cases} \quad (7)$$

(2) Control Algorithm with Dead Zone

In computer control systems, in order to avoid too frequent control actions and eliminate oscillations caused by frequent actions, some systems can adopt control with dead zones.

$$f'(g)=\begin{cases}0.1 & when|f(g)|\le f_0\\ f(g) & when|f(g)|>f_0\end{cases} \quad (8)$$

In the formula, the dead zone f_0 is an adjustable parameter, and its specific value can be determined by experiment according to the actual control object.

(3) Integral Separation Control Algorithm with Dead Zone

Considering the advantages of the integral separation control algorithm and the control algorithm with dead zone, this paper proposes an integral separation control with dead zone, which is written in incremental form as the integral separation control algorithm with dead zone. The formula is;

$$\Delta v(g) = g_q * [f'(g) - f'(g-1)] + \lambda g_1 * f'(g)] \quad (9)$$

$$\Delta v(g) = g_w * [f'(g) - 2f'(g-1) + f'(g-2)] \quad (10)$$

In the formula, g is the reference value and f is the degree of control. According to the above analysis, the algorithm flow of the integral separation control algorithm with dead zone can be obtained [20].

2.2. Introduction to the Types of $Al_2O_3 - SiC - C$ Refractory Materials

$Al_2O_3 - SiC - C$-quality refractory materials can be roughly divided into shaped ASC-type refractories according to the manufacturing process (such as $Al_2O_3 - SiC - C$ brick: refers to a carbon composite refractory material that uses alumina and carbon as raw materials and is press-formed after being mixed with an organic binder) and unshaped $Al_2O_3 - SiC - C$-refractory Materials (such as $Al_2O_3 - SiC - C$ castables, ramming materials, spray materials, etc. in the iron ditch material). The $Al_2O_3 - SiC - C$ brick is a carbon composite refractory material with alumina, silicon carbide and carbon raw materials as the main components and phenolic resin as the main binder, as shown in Figure 4. Among them, alumina materials are mainly introduced in the form of high alumina bauxite clinker, fused corundum or sintered corundum. In the actual production and application process, the appropriate alumina material is selected according to the use conditions. According to the different content of SiO_2, silicon carbide materials can generally be divided into black silicon carbide and green silicon carbide. Black silicon carbide has good physical and chemical properties and low cost of use, so it is selected as the main refractory material application. Silicon carbide is a raw material source, and is usually added in the form of granules or fine powder. Graphite is used as the main carbon raw material for $Al_2O_3 - SiC - C$ bricks. On the one hand, it can improve the thermal shock performance of the material. On the other hand, the introduction of graphite increases the wetting angle between the working surface of the ASC brick and the slag, which prevents the slag from flowing into the $Al_2O_3 - SiC - C$ brick [21].

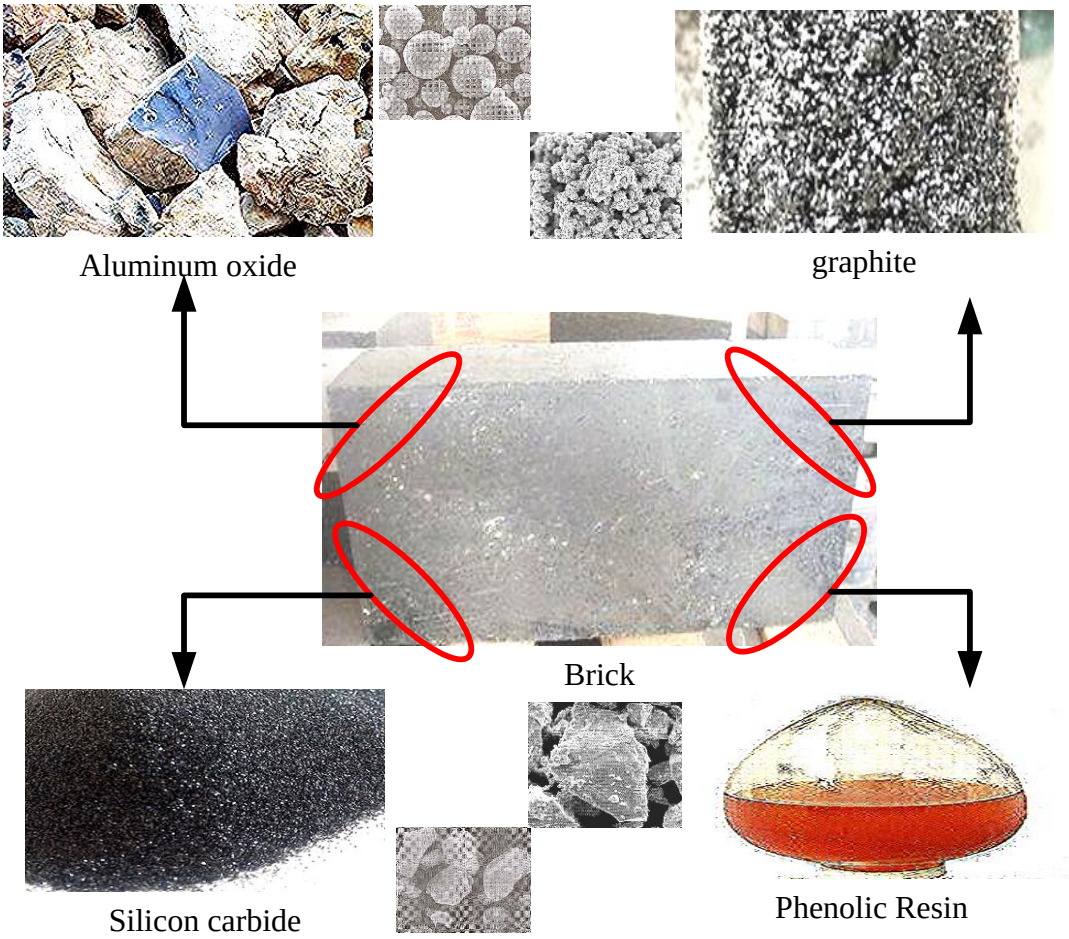

Figure 4. The brick of $Al_2O_3 - SiC - C$ refractory

It can be seen from Figure 4 that as a refractory material for molten iron transportation and pretreatment, $Al_2O_3 - SiC - C$ shaped products are used in molten iron transportation equipment such as molten iron tanks, torpedo mixers, and molten iron pretreatment equipment. Whether it is a hot metal ladle or a torpedo tank, when the molten iron is transported, the lining refractories will face the erosion and abrasion of the hot molten iron and the thermal stress generated by the severe thermal shock when the molten iron is poured, and must withstand the erosion and penetration of the molten iron and slag during the transportation. And the oxidation in the air at high temperature, after unloading, the temperature of the lining will drop sharply and thermal oxidation will occur again when exposed to the air. In the process of repeated loading, unloading and transportation, the lining refractory material needs to withstand a series of damage tests such as scouring and abrasion, slag corrosion, thermal spalling, and air oxidation. The torpedo tank also involves the hot metal pretreatment process, that is, the three dephosphorization (dephosphorization, desulfurization, and desiliconization) treatment processes. The torpedo tank in the hot metal pretreatment process is not only subject to the erosion, erosion, and penetration of hot metal, but also the severe erosion of metallurgical auxiliary materials during the three-off process. A large number of test results show that the $Al_2O_3 - SiC - C$-shaped product exhibits excellent corrosion resistance to the solvent or slag generated in the molten iron during the hot metal pretreatment process. At the same time, it has high thermal shock resistance and can withstand the continuous erosion of the molten iron. During

the process, it can resist the structural delamination and peeling caused by the infiltration of slag and the reaction of the slag and the material layer. It is the most ideal lining material in the process of molten iron transportation and pretreatment, and can meet the requirements of strict working environment. At the same time, it has a long service life [22]. Therefore, from the mid-to-late 1980s to the present, $Al_2O_3 - SiC - C$-bricks have been used as the main working lining material on hot metal ladle and torpedo tanks.

$Al_2O_3 - SiC - C$ Unshaped refractories, the main components are also alumina, silicon carbide and carbon raw materials. Calcium aluminate cement, clay, phosphate or other sol type liquids are usually used as binders. It is generally used to make iron ditch, hot metal ladle and other lining refractory materials. As shown in Figure 5, the $Al_2O_3 - SiC - C$-unshaped refractory material is used in the blast furnace tapping site and its preforms.

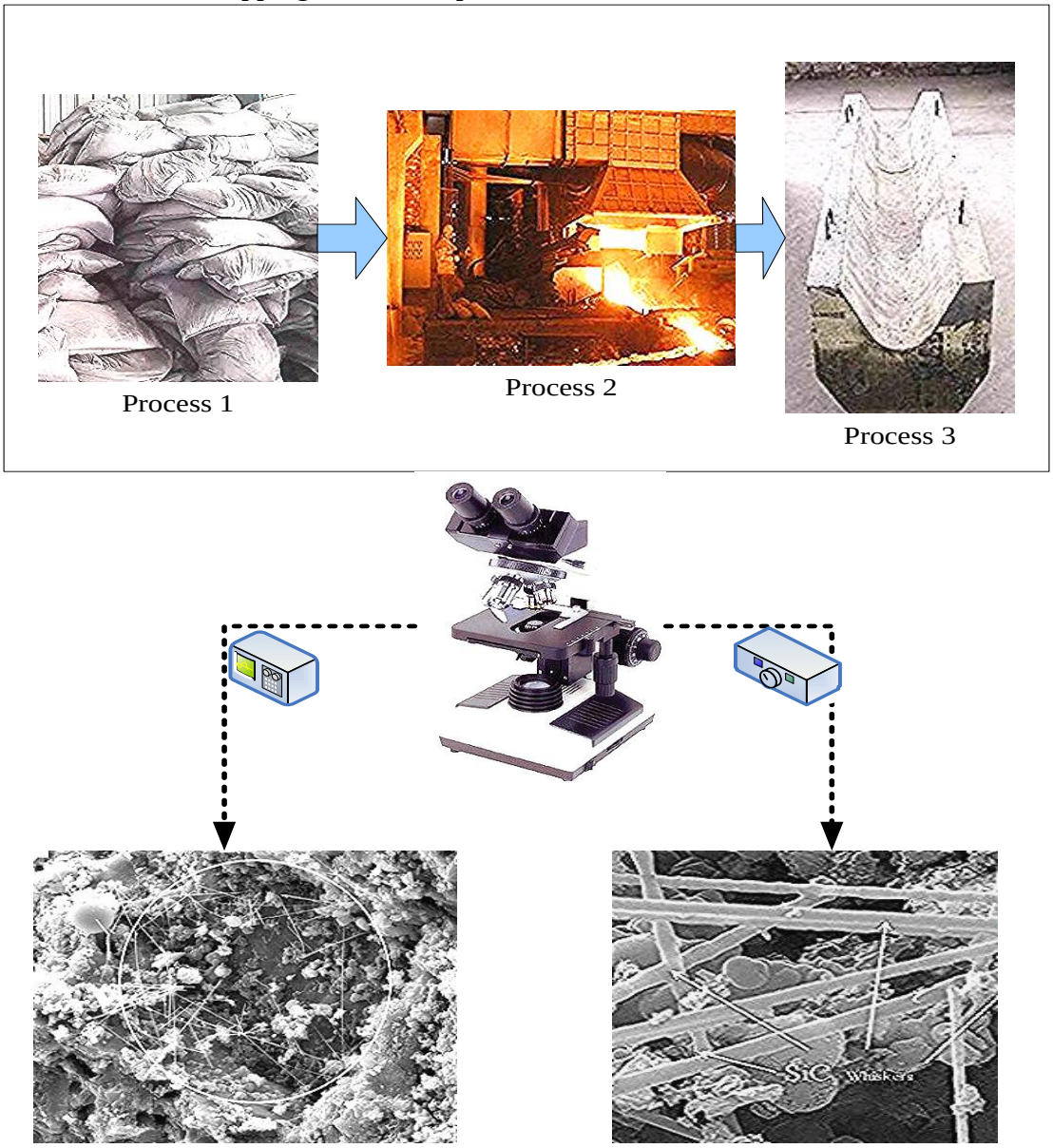

Figure 5. The blast furnace iron groove and its casting product

It can be seen from Figure 5 that according to different preparation methods, $Al_2O_3-SiC-C$-shaped refractories can be divided into many varieties such as ramming material, dry vibrating material, castable material, repair/gunning material, and tapping mud [23].

In recent years, $Al_2O_3-SiC-C$-type castable refractories have been widely used in the steel industry due to their good performance and successful commercial promotion. Among them, the Al_2O_3 material has high mechanical strength and corrosion resistance. SiC and carbon raw materials have good thermal conductivity, low expansion coefficient and non-wetting with slag. The combination of SiC and C can improve the material. The oxidation resistance can also prevent the slag from penetrating into the matrix. Pure calcium aluminate cement (65%~75% Al_2O_3, 25%~35%CaO) is widely used as a binder for $Al_2O_3-SiC-C$-type castables because of its low content of CaO and less impurities, while improving the performance of products. The dispersant can not only maintain the good construction fluidity of the castable, but also play a role in adjusting the hardening time for a certain period. Commonly used dispersants for iron hook castables include phosphates, inorganic salts and other organic chemical dispersants. In addition, in order to improve the dispersion effect, several dispersants can be used to compound them into composite dispersants. Figure 6 shows the research and development process of $Al_2O_3-SiC-C$-quality amorphous refractories.

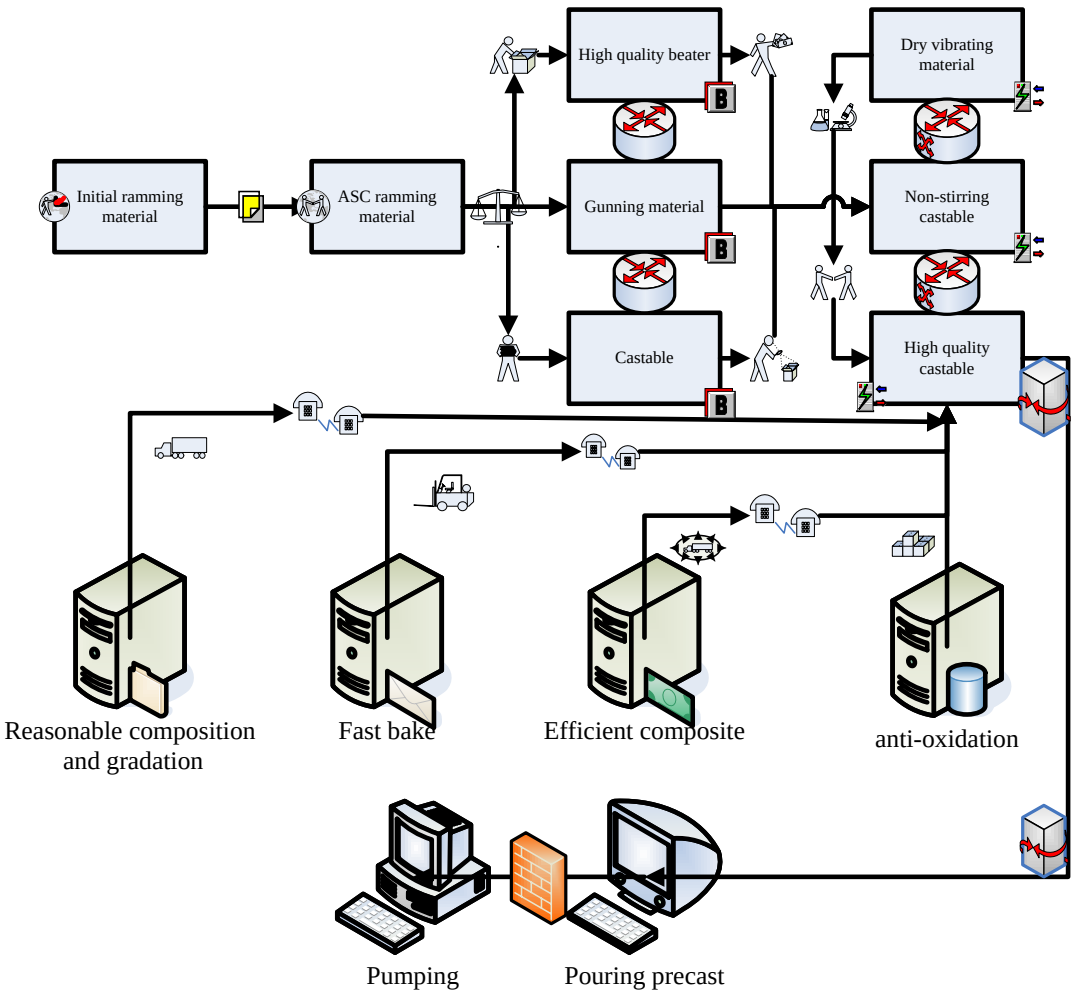

Figure 6. Development process of $Al_2O_3-SiC-C$ refractory

From Figure 6, we can see that with the advancement of smelting technology, the efficiency of the blast furnace has been greatly improved, and the output has also been significantly improved. The friction and corrosion of cast iron and slag will affect the refractory materials for iron ditch. Therefore, we have done a lot of research on the solder materials used in the water outlet channel, and have produced a variety of non-slip materials, which are used in different construction materials for subway trenches [24].

2.3. Iron Trough Castables and Mathematical Model of Steel

Rheology is a branch that studies the deformation and flow of a system under external influences. The performance of the overall structure of refractory materials is closely related to the flow of materials, and the performance efficiency has a decisive influence on the quality of the product. Refractory castables are usually composed of various additives with better performance, fine powder and micro powder (extremely fine powder), fine and coarse particles, water or mixed water. For refractory castables, if the work can be studied and discussed from the perspective of rheology, it is of great significance for improving construction efficiency and product performance.

In the field of unshaped refractories, for the system composed of coarse particles-powder-water, particle gradation is one of the important factors affecting its rheological properties; while the powder-water suspension system affects its rheological properties There are many factors, mainly including the particle size distribution of the powder, the solid phase volume fraction of the system, the type and amount of dispersant, the pH value, and the ambient temperature.

(1) Aggregate Particle Gradation

In the field of refractory castables, particle size control is an important research content, which not only affects the microstructure and performance of the castable, but also has an important impact on the construction performance. In the slurry, coarse particles (particle size greater than 5mm) have poor fluidity, while fine particles and micropowders have good fluidity. Therefore, when the system contains more large particles, casting molding is often difficult [25]. The distribution equation is:

$$zqls = \left(\frac{w}{w_i}\right)^m + \left(\frac{d}{d_s}\right)^p + \left(\frac{y}{y_b}\right)^a \quad (11)$$

In the formula: ZQLS is the percentage of particles with a diameter smaller than W; W_i is the maximum particle size; m is the particle size distribution coefficient. The smaller the m value, the more fine powder contained in the material. The fine powder can fill the gaps between the particles, and at the same time play a certain lubricating effect and improve the fluidity of the slurry. Table 2 lists the basic physical properties of some commonly used reinforcement particles.

Table 2. Mechanical properties of common used reinforce particles

Reinforcing particles	Hardness	Modulus	Density
C	62	990	3.3
ZrB_2	31	410	5.98
SiC	25	400	3.3
Si_3N_4	16	280	3.4
Al_2O_3	15	350	4.01

(2) Solid Phase Volume Fraction

In the field of unshaped refractory materials, the product should have good performance, and the amount of water added during casting should be minimized, that is, a slurry with a high solid content should be prepared, which often results in a slurry with a larger viscosity and difficult to shape.

$$\frac{\mu}{\mu_{\mathrm{n}}}=\left(1-\frac{\gamma}{\gamma_{n}}\right)^{-(\mu)\gamma_{n}}+\left(1-\frac{\beta}{\beta_{\mathrm{n}}}\right)^{-\lambda_{\mathrm{n}}} \tag{12}$$

In the formula, μ is the viscosity of the slurry, μ_{n} is the viscosity of the dispersion medium, and γ_{n} is the maximum solid phase volume fraction,

In fact, the dispersed phase of most suspensions is "soft particles", that is, there is interaction before the particles are in contact with each other.

$$\gamma_{\mathrm{fll}}=\gamma\left(1+\frac{\theta}{x}\right)^{2.5}+\vartheta\left(2+\frac{\pi}{\rho}\right)^{\frac{1}{3}} \tag{13}$$

For spherical particles with an adsorption layer thickness of θ and a particle radius of x, the rheological behavior of a stable soft sphere system is very similar to that of rigid particle fluids. However, because soft particles have a wider range of electrostatic repulsion, the change in solid content has an effect on viscosity.

(3) The Dispersant

In particle dispersion technology, dispersants play an important role, and the ways to achieve particle dispersion include the following: ①surface adsorption; ②reaction; ③coating or coating, etc. The dispersion object of refractory castable is a system composed of inorganic powder and water. The selected dispersant not only has good compatibility and compatibility with water, but also has a strong effect on inorganic powder.

(4) The PH Value

The purpose of adjusting the pH value is to increase the electrostatic repulsion between particles by changing the chargeability of the powder surface, thereby improving the dispersion of the slurry. The flow stress of a material characterizes the resistance to plastic deformation of the material, and has nothing to do with the stress state. Generally, it can be expressed as a function of temperature, rate and degree of deformation;

$$\theta=\theta\left(\mathrm{a}\%,s,\gamma,\dot{\gamma}^{*},s\right)+\pi\left(x\%,t,\beta\right) \tag{14}$$

Its incremental form is;

$$\mathrm{w}\theta=\frac{\rho\theta}{\rho a}wa+\frac{\rho\theta}{\rho s}ws+\frac{\rho\theta}{\rho\gamma}w\gamma+\frac{\rho\theta}{\rho\kappa}w\kappa+\frac{\rho\theta}{\rho\eta}w\eta \tag{15}$$

Because equation (15) is difficult to solve, in practice, experiments are usually used to establish mathematical statistical models to describe the relationship between flow stress and deformation parameters;

$$\theta=\mathrm{g}_{s}g_{o}g_{o}g_{t}\rho_{p}+e_{l}e_{f}e_{k}e_{g}\varpi_{c} \tag{16}$$

$$\theta=x\rho^{x}\&^{y}uzi\left(-zs\right)+\sum_{y_{b}}^{c_{t}}x_{a} \tag{17}$$

After the above model is improved;

$$\theta = \theta_0 \left(\frac{\rho}{4} \right)^{y_1 s + y_2} uzi\left(y_3 \frac{s}{900} + y_4 \right) \quad (18)$$

$$\rho_0 = \mathrm{x}\varpi^{y} \varpi^{z} uzi\left[\left(\frac{s}{w} \right)^{n} - \frac{(\varpi + g)}{o} \right] \quad (19)$$

$$\rho_1^{*} = \varpi uzi\left(\frac{m}{es} \right) + \cos g\left(\frac{\varpi}{g} \right) \quad (20)$$

$$\psi = \left[\mathrm{y}_6 \left(\frac{\rho}{4} \right)^{y_3} - (y_5 - 1)\left(\frac{\rho}{4.5} \right) \right] \quad (21)$$

ψ is the deformation flow stress model, which can improve the prediction accuracy of flow stress during plastic processing of materials,

3. Method Experiments and Conclusions Based on the Influence of Carbon Raw Materials on the Properties of $Al_2O_3 - SiC - C$ Iron Trough Castable Materials

3.1. Experimental Materials

The main raw materials for the test include tabular corundum, silicon carbide, carbon, activated alumina powder, SiO_2powder, Al-Si alloy powder, metal Si powder, and calcium aluminate cement as the binder. The main raw materials used in this article are listed in Table 3.

Table 3. Experimental reagents and materials

Serial number	raw material	Portion%	Specification	Origin
1	Tabular corundum	65.4	EM1.0	Anmai Aluminum
2	Silicon carbide	22.1	AR1.1	Anmai Aluminum
3	Spherical pitch	3.6	XE3.0	Tianjin Kainos
4	Activated alumina powder	0.8	IN2.0	BASF
5	Calcium aluminate cement	8.1	QW4.0	Licheng Reagent Factory

The sample configuration is shown in Table 4.

Table 4. The composition of $Al_2O_3 - SiC - C$ castable specimens

Raw material(wt%)	X	Y	Z	W
Tabular corundum	54	52	51	50
SiC	16	15	16	15
Spherical pitch	0.5	2.5	4	6
Al_2O_3	9	9.5	10.5	9
SiO_2	3.5	3.8	4.2	4.1
Al-Si alloy powder	1.6	1.5	1.7	1.8
$3CaO \cdot Al_2O_3$	0.25	0.22	0.18	0.26

Weigh according to the ratio in Table 4. After the aggregate and fine powder are prepared according to the predetermined ratio, put the fine powder into the sand mixer for pre-mixing, and then put the aggregate into the mixing pot during the mixing process. Finally, the sample was heat-treated at 1000 ℃ and 1350 ℃ for three hours in a buried coke atmosphere.

3.2. Experimental Equipment

The main equipment used in the experiment of this paper is shown in Table 5.

Table 5. The experimental instruments

Equipment name	Model	Origin	Credibility
Rotating viscometer	OAT-10X	China Chengdu Instrument Factory	99.6%
Fully automatic true density analyzer	PYC1220	American mike co., ltd.	99.8%
Laser particle size analyzer	NT1800	Malvern Instruments	99.7%
Potentiometer	PROBR3.0	Colloidal Dynamics, USA	99.8%
Blender	KK-4	Zhengzhou, China	99.6%
Density tester	AMH-2.5X	China	99.8%
Experimental instrument	WGC-4800	China	99.9%
High temperature electric furnace	HTI600	Luoyang, China	99.7%

3.3. Experimental Method

The ingredients were prepared according to the formula shown in Table 4, premixed for 3-4min, then dry-mixed in a cement mortar mixer for 0.5min, then poured into the solution with dispersant added according to the formula ratio, and continued wet-mixing for 5min. After the castable has good fluidity, it is poured into a 35mmx35mmx 145mm triple mold for vibration molding. Curing

the formed sample at room temperature for 20 hours, and then demold. Then, the sample was placed in a blast drying oven at 105 ℃ to dry for 21 hours, and after taking it out, it was heat-treated at 700 ℃, 1050 ℃, and 1500 ℃ for 2.5 hours, respectively. Finally, measure the linear change rate, bulk density and apparent porosity, normal temperature flexural strength and compressive strength after heat treatment at different temperatures. Measure the high-temperature flexural strength at 1500*Cx25min after 1500*Cx2.5h treatment and the retention of residual flexural strength of each sample that was air-cooled three times at 1050 ℃.

The preparation of the matrix sample is similar to that of the castable. After the materials are mixed, the dispersant solution is added and stirred to form a slurry, which is treated according to the curing, drying and heat treatment system of the castable sample. In order to explore the relationship between the influence of carbon raw materials and added amount on the properties of the castable and the phase composition and microstructure of the castable matrix, X-ray diffractometer and scanning electron microscope were used to analyze the effect of carbon raw materials and added amount on the castable matrix.

3.4. Result Analysis

Figure 7 shows the X-ray diffraction (XRD) images of two sets of samples with 0.8% and 6.8% carbon added after heat treatment at 1050 ℃ and 1500 ℃.

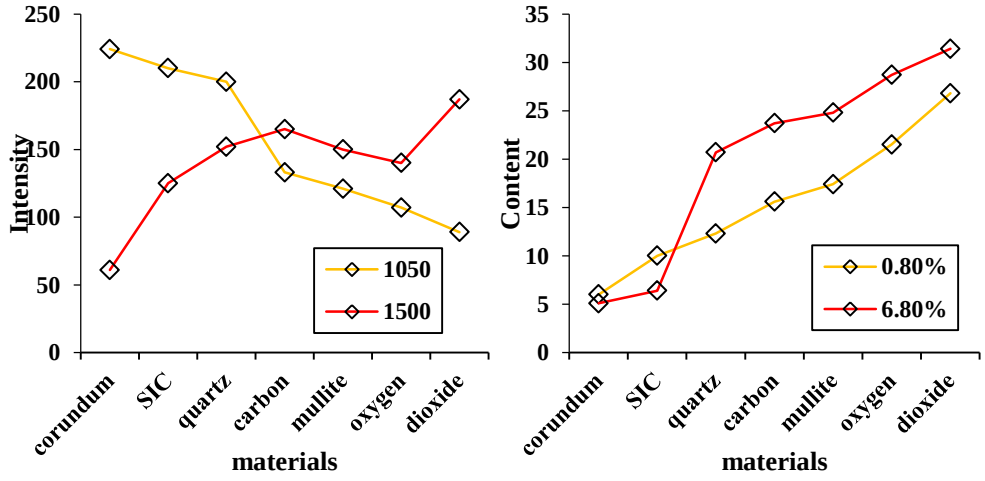

Figure 7. XRD patterns of samples after heat treatment at different temperatures

It can be seen from Figure 7 that the main crystalline phases of the X group samples with a carbon content of 0.8% and the W group samples with a carbon content of 6.8% are both corundum and SiC, which are derived from raw materials, and carbon is formed after carbonization at high temperature. Quartz phase and mullite phase with weaker carbon and diffraction peaks. The two groups of samples burned at 1050 ℃ have the same phase composition. The mullite diffraction peak of the sample with 6.8% carbon content is slightly higher than that of the sample with 0.8% carbon content. After heat treatment at 1500℃, the sample with 6.8% carbon content has a higher SiC main peak than the sample with 0.8% carbon content, indicating that as the carbon content increases, the carbon content of the sample after carbonization at high temperature is also As it increases, more SiC is formed in the sample.

The microstructures of the four groups of samples (X, Y, Z, W) with different amounts of carbon added after heat treatment at different temperatures are shown in Figure 8.

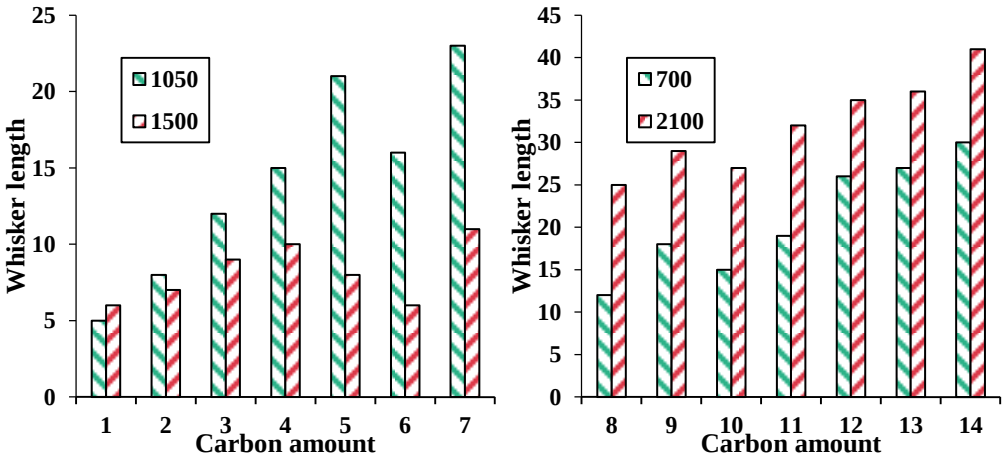

Figure 8. Microstructure analysis of castable sample

It can be seen from Figure 8 that when the heat treatment temperature is 1050 ℃ and the carbon addition amount is 1.2%, the sample has a low carbon content and volatiles escape during the high-temperature carbonization process, resulting in the carbon becoming an amorphous carbon structure at high temperatures. There are few transformation variables, and the change of the microstructure of the relative material is not obvious. When the amount of carbon added was increased to 2.8% and 4.7%, carbon microspheres appeared in the sample, and the more carbon content, the amount of spheres increased, and the particle size of the microspheres also increased. When the carbon content is continuously increased to 6.8%, relatively straight carbon nanotubes with a hollow tubular shape appear inside the sample. The in-situ generated CNTs have a longer aspect ratio, and the whisker length is between 13-28um and the diameter distribution is uniform. . At 1500 ℃, it can be seen that the four groups of samples with different amounts of carbon added have formed SiC whiskers in-situ after high temperature heat treatment. In the sample with 1.2% carbon addition, a small amount of incompletely developed SiC whiskers are formed, and the amount of whiskers generated is small and the length and diameter are relatively low. When the amount of carbon added is 2.8%, a certain amount of well-developed SiC whiskers are generated inside the sample, the whiskers are distributed in the pores, the length and diameter are relatively low, and the morphology is short fiber. When the addition of carbon is increased to 4.7%, there are well-developed SiC whiskers formed in-situ in the castable sample. The whisker aspect ratio is 18-44, and the thickness is relatively uniform without obvious defects. When the amount of carbon added reaches the maximum of 6.8%, it can be clearly seen that more whiskers are formed and the morphology develops better.

3.5. Performance Analysis

Figure 9 shows the vibration flow values of four groups of castable samples with different carbon additions.

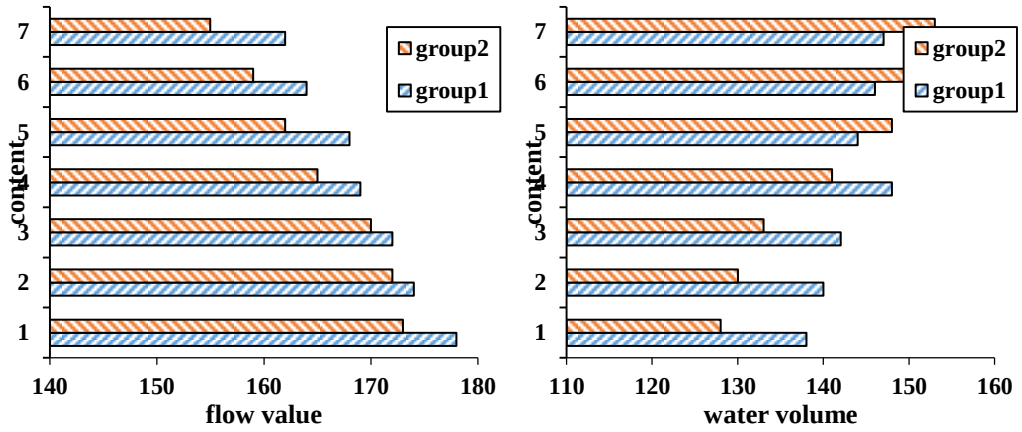

Figure 9. The influence of spherical pitch addition on the flow value of the sample

It can be seen from Figure 9 that as the amount of carbon added increases, the flow value of the castable decreases slightly from 180 to 162, and the overall castability of the sample is better. Carbon has a large water absorption rate. When the amount of water added is fixed, the amount of water available for pouring for samples with more carbon content shows a decreasing trend from 155 to 140, and the more voids generated by the accumulation of carbon, which causes the castable to vibrate and flow Decline in value.

Figure 10 shows the high temperature flexural strength of the sample after heat treatment at 1500℃,

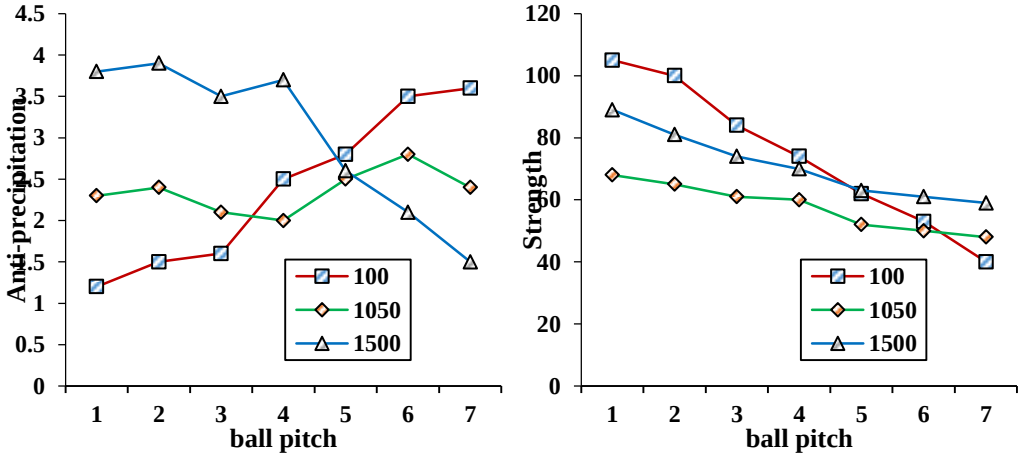

Figure 10. Hot Modulus of Rupture of samples with different content of ball pitch

It can be seen from Figure 10 that as the amount of carbon added increases, the high temperature flexural strength of the sample has increased. When the carbon addition amount is 4.7%, the high temperature flexural strength of the sample has a maximum value of 2.8MPa. When the carbon content is increased to 6.8%, the high temperature flexural strength of the sample is decreasing. This is because as the amount of carbon added increases, the amount of residual carbon in the sample after carbonization at high temperature increases, and the more ceramic bonding phases are generated; with the increase of the carbon content in the sample, SiC whiskers are formed in situ in the sample, and the ceramic is bonded. With the addition of excessive carbon, more pores are left after the sample is carbonized, and more defects are introduced, which leads to loose internal

structure and cracks, which reduces the high-temperature mechanical properties of the material.

4. Discussion

Under the condition of buried carbon, with the increase of carbon addition, after 1050℃ heat treatment, $Al_2O_3-SiC-C$ castable sample contains tubular carbon nanotubes with high aspect ratio. When the sintering temperature is increased to 1500℃, the castable SiC whiskers are formed in-situ inside, and as the carbon content increases, the whiskers develop better, the aspect ratio increases, and the whisker content increases. With the increase of the amount of carbon added, the apparent porosity of drying and pouring decreased, and the apparent porosity of the samples after heat treatment at 1050 ℃ and 1500 ℃ increased significantly, and the bulk density decreased. With the increase of the amount of carbon added, the normal temperature flexural strength and normal temperature compressive strength of the samples under the same heat treatment temperature gradually decrease. The samples with the same carbon content increase from 1050 ℃ to 1500 ℃ as the heat treatment temperature. The mechanical strength has been improved. The increase of carbon addition is helpful to improve the high temperature flexural resistance of the $Al_2O_3-SiC-C$ castable sample. In this experiment, the high temperature flexural strength of the sample with 4.7% carbon reaches the maximum. The in-situ generated CNTs and SiC whisker ceramic phase work together to improve the mechanical properties of $Al_2O_3-SiC-C$ castables at room temperature and high temperature. As the amount of carbon added increases, the retention of residual compressive strength of the sample after three thermal shock tests shows a downward trend. In this experiment, the higher the carbon content, the worse the thermal shock stability of the sample.

5. Conclusion

This article mainly uses tabular corundum, silicon carbide, carbon raw materials, activated alumina powder, and alloy powder as raw materials, and uses pure calcium aluminate cement as a binder to prepare $Al_2O_3-SiC-C$ castables, and explores the role and influence of carbon raw materials. . In order to achieve the purpose of the research, this paper applied many scientific methods such as practical methods, found the instruments and reagents for experimenting, and at the same time studied the vibration flow value of four groups of castable samples with different amounts of carbon added. As the amount of carbon added increases, the flow value of the castable decreases slightly from 180 to 162. The amount of water available for pouring of the sample with more carbon content shows a decreasing trend from 155 to 140, which indicates that the overall pouring property of the sample is better, and it also shows that the more carbon content is not the better, when it exceeds a certain critical value At times, it will be counterproductive. The shortcomings of this article are: First, the integration of management and control is the development trend of enterprise production automation and management modernization. Realize the integration of management and control, realizing the sharing of on-site information resources and the rational use of resources. This article is relatively scarce in this area; secondly, in the future, research on castables under extreme loading conditions such as high strain rates should be carried out in order to reveal the pouring more deeply. Therefore, this is also the key to breakthrough in the future of this article. After all, the construction industry has higher requirements for operation accuracy, and strives to apply this article to actual operations as soon as possible.

Funding

This article is not supported by any foundation.

Data Availability

Data sharing is not applicable to this article as no new data were created or analysed in this study.

Conflict of Interest

The author states that this article has no conflict of interest.

References

[1] Papailias F , Thomakos D D , Liu J . The Baltic Dry Index: cyclicalities, forecasting and hedging strategies. Empirical Economics, 2017, 52(1):255-282. https://doi.org/10.1007/s00181-016-1081-9

[2] Hasa B , Martino E , Vakros J , et al. Front Cover: Effect of Carbon Support on the Electrocatalytic Properties of PtRu Catalysts (ChemElectroChem 19/2019). ChemElectroChem, 2019, 6(19):4917-4917. https://doi.org/10.1002/celc.201901388

[3] Fayomi O , Popoola A , Olorunniwo O E . Structural and properties of Zn-Al 2 O 3 -SiC nano-composite coatings by direct electrolytic process. The International Journal of Advanced Manufacturing Technology, 2016, 87(1-4):389-398. https://doi.org/10.1007/s00170-016-8428-4

[4] Pugalenthi P , Jayaraman M , Subburam V . Study of the microstructures and mechanical properties of aluminium hybrid composites with SiC and Al2O3. Materiali in Tehnologije, 2019, 53(1):49-55. https://doi.org/10.17222/mit.2018.118

[5] Shivakumar H , Renukappa N M , Shivakumar K N , et al. The Reinforcing Effect of Graphene on the Mechanical Properties of Carbon-Epoxy Composites. Open Journal of Composite Materials, 2020, 10(2):27-44. https://doi.org/10.4236/ojcm.2020.102003

[6] Shuaizhen L I , Bin L I , Qin L I , et al. Effect of carbon fillers on the conductive properties of polyurethane elastomer. Journal of Functional Materials, 2017, 48(8):08079-08084.

[7] P. W U , Liu S C , Jiang X R . Effect of multi-walled carbon nanotube addition on the microstructures and mechanical properties of Ti(C,N)-based cermets. Journal of Advanced Ceramics, 2018, 7(01):60-65. https://doi.org/10.1007/s40145-017-0256-y

[8] Knyazheva O A , Baklanova O N , Lavrenov A V , et al. The Effect of Mechanical Activation on the Physico-Chemical Properties of Carbon Black and Rubber Mixtures Filled with It. Journal of Siberian Federal University Chemistry, 2018, 11(4):552-563. https://doi.org/10.17516/1998-2836-0099

[9] Yang S , Xiao G , Ding D , et al. Effect of in-situ carbon containing calcium aluminate cement on properties of Al 2 O 3 -SiC-C based trough castables. Journal of Asian Ceramic Societies, 2020, 8(1):1-8.

[10] Tian X , Ding D , Zhang P , et al. Effect of andalusite with different particle sizes on properties of Al_2O_3-SiC-C castables. Naihuo Cailiao/Refractories, 2018, 52(6):422-425.

[11] El-Khatib S , Shash A Y , Elsayed A H , et al. Effect of Carbon Nano-Tubes, Micro and Nano Dispersions of SiC and Al2O3 on the Mechanical and Physical Properties of Pure Copper. Reviews on Advanced Materials Science, 2017, 52(1):126-133.

[12] X Peng, Huang Y , X Sun, et al. Effect of chromium coated carbon fiber on the thermal and mechanical properties of Cr@Gf/Cr@CF/AI composites. Journal of materials science, 2019, 30(8):7226-7233. https://doi.org/10.1007/s10854-019-01014-8

[13] Xu X , Li Y , Wang Q , et al. Effect of Alumina-Coated Graphite (ACG) on the Microstructure and Mechanical Properties of Al2O3-C Refractories. Journal of Ceramic Science & Technology, 2016, 8(4):455-462.

[14] Liu G , Yawei L I , Liao N , et al. Effect of B4C Additive on Microstructure and Mechanical Properties of Low Carbon Al2O3–C Refractories. Kuei Suan Jen Hsueh Pao/ Journal of the Chinese Ceramic Society, 2017, 45(9):1340-1346.

[15] Ding D , Chong X , Xiao G , et al. Combustion synthesis of B4C/Al2O3/C composite powders and their effects on properties of low carbon MgO-C refractories. Ceramics International, 2019, 45(13):16433-16441.

[16] Tian X , Liu G , Shang X , et al. Effect of carbon-coated Al 2 O 3 powder on structure and properties of low-carbon MgO-C refractory composites. Processing and Application of Ceramics, 2018, 12(3):295-302. https://doi.org/10.2298/PAC1803295T

[17] Liu G , Liao N , Nath M , et al. Optimized mechanical properties and oxidation resistance of low carbon Al 2 O 3 -C refractories through Ti 3 AlC 2 addition. Journal of the European Ceramic Society, 2021, 41(4):2948-2957.

[18] Feng X , Sza B , Zhuang M , et al. Effect of TaSi 2 /ZrSi 2 on ablation properties of carbon-phenolic composite irradiated by high-intensity continuous laser. Ceramics International, 2020, 46(18):28443-28450.

[19] Zhe W , Yue L , Bzab C , et al. Mechanical properties and microstructure of Al 2 O 3 -SiC w ceramic tool material toughened by Si 3 N 4 particles. Ceramics International, 2020, 46(7):8845-8852. https://doi.org/10.1016/j.ceramint.2019.12.129

[20] Liu C , Li W , Meng J , et al. Relationship between microstructure and torsional properties of Qst32-3 ultra-low carbon steel. Jinshu Rechuli/Heat Treatment of Metals, 2017, 42(2):76-79.

[21] Jie Z , Tza B , Yong C , et al. Fabrication and mechanical properties of ZrO2–Al2O3–SiC(w) composites by oscillatory pressure sintering - ScienceDirect. Ceramics International, 2020, 46(16):25719-25725.

[22]Gocmez, Hasan, Yeniceri, et al. The Influence of SiC, B4C and ZrO2 on the densification and mechanical properties of ZrB2. Journal of the Australasian ceramic society, 2016, 52(2):73-75.

[23] Shaw S , Yuan B , Tian X , et al. Building Materials from Colloidal Nanocrystal Arrays: Preventing Crack Formation during Ligand Removal by Controlling Structure and Solvation. Advanced Materials, 2016, 28(40):8892-8899. https://doi.org/10.1002/adma.201601872

[24] Ondova M , Estokova A . Environmental impact assessment of building foundation in masonry family houses related to the total used building materials. Environmental Progress & Sustainable Energy, 2016, 35(4):1113-1120. https://doi.org/10.1002/ep.12307

[25]Tingting, Feng, Xinwei, et al. Natural radioactivity, radon exhalation rate and radiation dose of fly ash used as building materials in Xiangyang, China. Indoor and Built Environment, 2016, 25(4):626-634. https://doi.org/10.1177/1420326X15573276